Stem Cell Research & Therapy

RESEARCH

Open Access

Mesenchymal stem cells-derived exosomes attenuate mouse non-heart-beating liver transplantation through Mir-17-5p-regulated Kupffer cell pyroptosis

Yang Tian[1†], Ming Jin[1†], Nanwei Ye[3†], Zhenzhen Gao[1], Yuancong Jiang[2*] and Sheng Yan[1*]

Abstract

Background Liver transplantation is the most effective treatment for end-stage liver disease. However, the shortage of donor livers has become a significant obstacle to the advancement of liver transplantation. Mesenchymal stem cells-derived exosomes (MSCs-Exo) have been extensively investigated in liver diseases. However, the underlying mechanisms of how they can protect organ donation after cardiac death (DCD) livers remain unclear.

Methods In this study, an arterialized mouse non-heart-beating (NHB) liver transplantation model was used to investigate the effect of MSCs-Exo on NHB liver transplantation. The survival rates, histology, pro-inflammatory cytokine and chemokine expression, and underlying mechanisms were investigated.

Results The infusion of MSCs-Exo reduced the injury to DCD liver graft tissue. In vitro and in vivo experiments demonstrated that MSCs-Exo could inhibit hydrogen peroxide-induced pyroptosis of Kupffer cells. We found that miR-17-5p was significantly abundant in MSCs-Exo, targeting and regulating the TXNIP expression. This action inhibited NLRP3-mediated pyroptosis of Kupffer cells through the classical Caspase1-dependent pathway, alleviating DCD liver graft injury.

Conclusion Our study elucidated a protective role for MSCs-Exo in a NHB liver transplantation model. This mechanism provides a theoretical basis and new strategies for the clinical application of MSCs-Exo to improve liver graft quality and alleviate the organ shortage in liver transplantation.

Keywords Donation after cardiac death, Liver transplantation, Ischemia/reperfusion injury, Mesenchymal stem cells-derived exosomes, Pyroptosis

[†]Yang Tian, Ming Jin and Nanwei Ye contributed equally to this work.

*Correspondence:
Yuancong Jiang
jiangyuancong@zju.edu.cn
Sheng Yan
shengyan@zju.edu.cn

[1]Department of Surgery, Second Affiliated Hospital of School of Medicine, Zhejiang University, Jie-Fang Road #88, Hangzhou, Zhejiang Province 310009, China
[2]Department of Surgery, Shaoxing People's Hospital, Zhejiang University School of Medicine, Zhong-Xing North Road #568, Shaoxing, Zhejiang Province 312000, China
[3]Department of Medical Research Center, Shaoxing People's Hospital, Zhejiang University School of Medicine, Shaoxing, China

Introduction

Liver transplantation is considered the final cure for end-stage liver disease. It is an extremely significant social need and holds a high status in China and worldwide. With the advancement of surgical technology and the development of immunosuppressants, the survival rate of liver transplantation has gradually increased. However, the problem of organ shortage has become more prevalent, significantly restricting the development of liver transplantation [1]. According to World Health Organization statistics, the global prevalence of patients with end-stage liver disease is 30 million. However, only 25,000 people receive liver transplants annually [2]. In China, approximately 8 million patients have end-stage liver disease; however, approximately 2,000 liver transplants are performed annually. A significant number of patients die because the disease worsens while waiting for a liver donor [3–5]. Organ donation after cardiac death (DCD) is the primary and most important source of organ donors worldwide. However, the number of liver donations remains significantly limited. Additionally, donor livers inevitably suffer ischemia-reperfusion injury (IRI) during DCD due to cardiac arrest and termination of effective circulation, which further exacerbates the shortage of donor livers [6, 7]. Several strategies, including hepatoprotective drugs and extracorporeal liver perfusion systems, have been implemented to reduce liver damage and improve the quality of DCD liver. However, the utilization rate of DCD liver remains limited, requiring the urgent exploration of more effective treatments in liver transplantation [8].

In clinical practice, DCD livers can tolerate cold storage for up to 24 h; however, it is difficult to withstand warm ischemia for more than 30 min. Prolonged warm ischemia causes the primary graft to become non-functional, requiring its disposal. This indisputable fact highlights the critical role of warm ischemia-reperfusion injury in determining the quality of liver donation [9, 10]. Multiple studies suggest that hepatic Kupffer cells are extensively involved in warm ischemia-reperfusion of the transplanted liver through pyroptosis to initiate immune response [11]. Pyroptosis is a form of inflammatory programmed cell death distinct from apoptosis. Pyroptosis is characterized by specific molecular features, including chromatin condensation, DNA fragmentation occurring independently of DNA damage, and the formation of membrane pores [12–14]. Kupffer cells are macrophages accounting for 30% of non-parenchymal cells in the liver. They contain the characteristic marker F4/80 on their surface and endogenously drive the NLRP3 inflammasome activation [15]. As pivotal sensor cells in the liver, Kupffer cells can promptly detect severe pathological stimuli and activate Caspase1 through NLRP3 inflammasome activation. This activation initiates the classic pyroptosis pathway, resulting in cell membrane rupture [16, 17]. This leads to the release of various inflammatory factors and chemokines, initiating a strong immune-inflammatory response crucial for regulating the liver's natural immunity, antagonizing inflammatory signals, and maintaining liver immune homeostasis [18]. After post-reperfusion, prolonged warm ischemia increases the production of reactive oxygen species and other damage-associated molecular patterns in the donor liver. Besides, the NLRP3 inflammasome produces a large amount of active Caspase1 and results in significant pyroptosis in Kupffer cells. With Caspase1 activation, the precursors of IL-1β and IL-18 are cleaved by the activated Caspase1, releasing multiple pro-inflammatory factors, including IL-1β, IL-18, TNFα, and CXCL1. This promotes the accumulation of inflammatory cells in the liver, resulting in rapid aggravation of inflammation and massive apoptosis of liver cells [6, 19]. Consequently, exploring effective treatments to reduce Kupffer cell pyroptosis induced by ischemia-reperfusion injury is the key to improving the quality of DCD liver donors and alleviating the shortage of liver donors [17, 19].

In the past two decades, mesenchymal stem cells (MSCs) have been reported to have potential effects in suppressing immune responses and reducing liver ischemia-reperfusion injury [20–22]. Since < 1% of MSCs can migrate to damaged target organs, it is generally accepted that MSCs restore organ damage primarily through paracrine effects [23–25]. Recently, researchers have discovered that mesenchymal stem cells-derived exosomes (MSCs-Exo) are the primary carriers mediating the paracrine effects of MSCs [26]. These exosomes are 40–150 nm in diameter and are released into to the extracellular matrix [27, 28]. These exosomes contain more than 850 gene products and 150 kinds of miRNAs, which can cross cell membranes and play important roles in cell communication, including regulating homeostasis, promoting repair, and reducing damage [29]. Gustafson and Lou et al. indicated that Kupffer cells in the liver participate in the cognitive and phagocytic functions of MSCs-Exo, thereby significantly improving LPS-induced acute liver failure [11, 30]. Moreover, Haga et al. investigated that MSCs-Exo promoted the repair of liver damage by regulating the function of macrophages [31]. However, due to the difficulty of animal liver transplantation models, current research on whether MSCs-Exo could protect DCD liver donors and its intrinsic mechanism remains unclear.

In this study, we used an arterialized mouse orthotopic DCD liver transplantation model to investigate the protective effect of MSCs-Exo on DCD livers [6]. We demonstrated that the infusion of MSCs-Exo reduced the injury to DCD liver graft tissue and pyroptosis of intrahepatic Kupffer cells. In vitro experiments exhibited

that MSCs-Exo inhibited hydrogen peroxide-induced pyroptosis of Kupffer cells. We found that miR-17-5p was highly abundant in MSCs-Exo. Both in vivo and in vitro experiments suggested that miR-17-5p in MSCs-Exo targeted and regulated TXNIP expression, inhibiting NLRP3-mediated pyroptosis of Kupffer cells through the classical Caspase1-dependent pathway, thereby alleviating DCD liver graft injury. The revelation of this mechanism provides a theoretical basis and new ideas for the clinical application of MSCs-Exo to improve the quality of liver grafts and alleviate the organ shortage in liver transplantation.

Materials and methods

Cells and reagents

The immortalized mouse-derived T40-MSCs were isolated and provided by Prof. Weimin Fan of Zhejiang University. The mouse macrophage cell lines RAW 264.7 (CL-0190) were obtained from the Wuhan Pricella Life Technology Co., LTD. Hydrogen peroxide (H_2O_2) (#88597) and $GdCl_3$ (#439770) was obtained from Sigma-Aldrich.

Animals

Male wild-type C57Bl/6 and CBF1 (8–10 weeks old) mice were obtained from the Shanghai Slack Laboratory Animal Center. All mice were kept in a specific pathogen-free environment. Generally, there were six mice per group, and a total of 180 mice were used. Mice were assigned to control and treatment groups with exosomes using a random number sequence method. All animal studies were approved by the Institutional Animal Care and Use Committee of Zhejiang Chinese Medicine University 2020 – 379.

The arterialized mouse non-heart-beating (NHB) liver transplantation model has been described previously [6]. Briefly, the model was established by anastomosis of the hepatic artery and the recipient's abdominal aorta. After carefully positioning the donor liver within the recipient's abdominal cavity, we sutured the liver's superior and inferior vena cava. The 'double cuff' technique was employed for the reconstruction of both the portal vein and the inferior vena cava, which allowed us to restore portal vein blood flow, thereby ending the cold ischemia and liverless phase. A biliary stent was utilized for bile duct reconstruction. Additionally, the donor liver's extended hepatic artery was anastomosed end-to-side to the recipient's iliac artery, ensuring the reestablishment of the liver's arterial blood supply. Cardiac arrest time was controlled by CO_2 asphyxiation to simulate warm ischemia during DCD donation. During the transplantation, the upper pole of the spleen was punctured, and 250 μg of MSCs-Exo in 50 μl of PBS was slowly injected into the spleen, returning to the liver through the portal venous system and sealing with electrocoagulation. In other experiments, donor C57Bl/6 mice were injected intraperitoneally with 20 mg/Kg of $GdCl_3$ solution 24 h before transplantation to eliminate intrahepatic Kupffer cells. The experimental animals were evaluated to rule out death due to surgical reasons. Generally, the death of mice is very frequent within 6 h of surgery. Then, the 14-day transplant recipient survival was observed and recorded every 6 h. This study did not adopt a blind method. The work has been reported in line with the ARRIVE guidelines 2.0.

Exosome isolation and identification

MSCs in the logarithmic phase were cultured with exosome-depleted fetal bovine serum (BS-1205, Opcel, China) for 48 h. After that, the supernatants derived from cultured MSCs were subjected to centrifugation at 300 g for 10 min, followed by 2000 g for 20 min at 4 °C, in order to eliminate cellular debris and shedding vesicles. The supernatants were then filtered through 0.22 μm membrane filters and further centrifuged at 110,000 g for 70 min at 4 °C. The supernatant was discarded, and the pellet was resuspended in 50 mL of PBS. This suspension underwent another round of centrifugation at 110,000 g for 70 min at 4 °C. The resulting exosomes were resuspended in PBS and stored at -80 °C for subsequent analyses.

The morphology of MSCs-Exo was observed using a 120 kV transmission electron microscope (Tecnai G2 spirit, Thermo FEI, Czech Republic). Then, 10 μl MSCs-Exo was diluted and measured using a flow nanoanalyzer (N30E, NanoFCM, China). Furthermore, the marker proteins CD81, HSP70 and TSG101 of MSCs-Exo were determined by western blotting.

Liver function assay and hematoxylin and eosin (HE) staining

After 6 h of transplantation, mice were anesthetized with pentobarbital (100 mg/kg) and sacrificed by cervical dislocation. Liver grafts and serum samples were harvested. The serum concentration of alanine aminotransferase (ALT) and aspartate aminotransferase (AST) were measured using an automatic biochemical analyzer (Hitachi, Tokyo, Japan). The liver samples were formalin-fixed and sectioned into 4 μm-thick slices. For histological staining, tissue sections were stained with HE and examined using optical microscopy.

Immunofluorescence analysis

For immunofluorescence analysis, the formalin-fixed cells were incubated with TXNIP (DF7506, Affinity, China) following the manufacturer's instructions. The liver sections were stained by F4/80 (GB113373, Servicebio, China) and Caspase-1 (GB11383, Servicebio, China)

Table 1 Primer sequences of mRNA used in detection for RT-PCR assay

Genes	Primer sequence (5′→3′)	
IL-1β	Forward	TGGACCTTCCAGGATGAGGACA
	Reverse	GTTCATCTCGGAGCCTGTAGTG
IL-2	Forward	GCGGCATGTTCTGGATTTGACTC
	Reverse	CCACCACAGTTGCTGACTCATC
IL-6	Forward	TACCACTTCACAAGTCGGAGGC
	Reverse	CTGCAAGTGCATCATCGTTGTTC
IL-18	Forward	GGACTGGCTGTGACCCTATC
	Reverse	TGTGTCCTGGCACACGTTTT
TNF-α	Forward	GGTGCCTATGTCTCAGCCTCTT
	Reverse	GCCATAGAACTGATGAGAGGGAG
IFN-γ	Forward	GAACTGGCAAAAGGATGGTGA
	Reverse	TGTGGGTTGTTGACCTCAAAC
β-actin	Forward	CATTGCTGACAGGATGCAGAAGG
	Reverse	TGCTGGAAGGTGGACAGTGAGG

Table 2 Primer sequences of miRNA used in detection for RT-PCR assay

Genes	Primer sequence (5′→3′)
mmu-miR-17-5p	GCGCAAAGTGCTTACAGTGCAGGTAG
mmu-miR-20a-5p	GCGCGTAAAGTGCTTATAGTGCAGGTAG
mmu-miR-223-5p	GCGCGTGTATTTGACAAGCTGAGTTG
mmu-miR-93-5p	CGCAAAGTGCTGTTCGTGCAGGTAG
mmu-miR-148a-5p	GCGCGAAAGTTCTGAGACACTCCGACT
mmu-miR-146a-5p	CGCGTGAGAACTGAATTCCATGGGTT
mmu-miR-16-5p	CGCGTAGCAGCACGTAAATATTGGCG

Table 3 Target sequence for knock down of miR-17-5p

Target	Target sequence (5′-3′)	Targeting location (InmRNA)
mMir17target-1	GAATAATGTCAAAGTGCTTAC	115,281,107–115,281,127 (pre)
mMir17target-2	GAAGCTGTGACCAGTCAGAAT	115,281,090–115,281,110 (pre)
mMir17target-3	CAGTCAGAATAATGTCAAAGT	115,281,101–115,281,121 (non-pre)

according to the manufacturer's protocol. The sections were visualized using a fluorescence microscope (Leica DMi8, Wetzlar, Germany).

Multiplex cytokine analysis and quantitative real-time polymerase chain reaction (RT-PCR)

The serum concentrations of cytokine and chemokine protein levels were measured through multiplex cytokine analysis (LX-MultiDTM-31, LabEx, China). The mRNA levels of the co-cultured Kupffer cells were determined through Real-Time Polymerase Chain Reaction (RT-PCR). The miRNA was extracted from MSCs-Exo using the Exosome RNA Purification Kit (EZB-exo-RN1, EZBioscience, China). The miRNA 1st Strand cDNA Synthesis Kit (by tailing A) (MR201, Vazyme, China) and Taq Pro Universal SYBR qPCR Master Mix (Q712, Vazyme, China) were used to test the relative content of miRNA. The primer sequences of mRNA and miRNA applied for RT-PCR are listed in Tables 1 and 2.

Lentiviral-shRNA transduction of miRNA-17-5p and transfection of TXNIP plasmids

PLKO.1-mMir17-shRNA-puro was synthesized by Antihela Biological Technology Trade Co. Ltd. to induce the miRNA-17-5p knockdown in MSCs (Table 3). The TXNIP plasmid was obtained from Vigene Biosciences (#231213001) to induce the TXNIP overexpression. The lentiviral-shRNA transduction of miRNA-17-5p and transfection of TXNIP plasmids were performed according to the manufacturer's protocol. The efficiency was determined through RT-PCR and western blotting analysis.

Western blotting analysis

The protein extracted from RAW 264.7 cells was used for detection. The NLRP3 (#15101, CST, USA), TXNIP (DF7506, Affinity, China), Cle-Caspase-1 (#89332, CST, USA), and GAPDH (#2118, CST, USA) proteins were analyzed through western blotting following the conventional protocol.

Cellular uptake of MSCs-Exo

To investigate the internalization of MSCs-Exo by Kupffer cells, the MSCs-Exo were labeled with DiI dye (#42364, Sigma-Aldrich, Germany) following the manufacturer's protocol. Subsequently, the DiI-labeled MSCs-Exo suspension underwent centrifugation at 110,000 g for 30 min at 4 °C. The supernatant was discarded, and the MSCs-Exo pellet was washed with 50 mL of PBS. This washing procedure was repeated 3 times to ensure the removal of any unbound DiI. Finally, the DiI-labeled MSCs-Exo were co-cultured with RAW264.7 cells at a concentration of 20 μg/mL. After 6 h, the cells underwent a washing procedure with PBS and were subsequently stained using DAPI (#C8054, Adamas life, China). The cells were finally analyzed and imaged using a confocal microscope (Zeiss, Germany). As a control, an equivalent volume of PBS was introduced into the RAW264.7 cells, in the absence of DiI-labeled MSCs-Exo.

Statistical analysis

Statistical analysis was performed using Statistical Package for Social Sciences (SPSS) software (version 25.0, SPSS Inc., Chicago, IL). The differences between the groups were compared using parametric one-way ANOVA and unpaired two-tailed Student's t-test. A P-value < 0.05 was considered statistically significant.

Significance was indicated by $^{*}P<0.05$, $^{**}P<0.01$, $^{***}P<0.001$, and ns (not significant) denotes $P>0.05$.

Results

Construction and optimization verification of mouse NHB liver transplantation model

The optimal mouse NHB liver transplantation model was first explored. Several different time points (0, 5, 10, and 20 min) were tested, with the sham operation group serving as a negative control. The 14-day survival of the mice after transplantation was observed. The results indicated that the survival rate of the sham group was 100%. However, as the NHB time increased, the 14-day survival rate of transplant recipients exhibited a significant downward trend (Fig. 1A). Then, we repeated the above animal model and obtained serum and liver tissue samples after the 6 h of NHB liver transplantation. Serological test results indicate that with the prolongation of NHB time, recipient mice's ALT and AST levels exhibited a significant upward trend 6 h after surgery. Furthermore, statistical analysis indicated that the ALT and AST expression levels exhibited no significant difference from NHB_{0min} until NHB reached 10 min or more (Fig. 1B and C). Besides, the HE results revealed that as the NHB time prolonged, the ischemic necrosis and vacuole-like changes in the transplanted liver significantly worsened (Fig. 1D). These results demonstrate that prolonged NHB time will cause significant damage to the donor's liver, leading to a significant increase in postoperative liver function damage and significantly reducing the recipient's 14-day survival rate after transplantation. Through data analysis of different NHB time points, it was found that postoperative liver function damage and mortality at 20 min after NHB were significantly severe. This observation is consistent with our clinical application, where the donor liver is seriously damaged due to the long warm ischemia time and would be discarded. The postoperative liver function injury and postoperative survival conditions at 0 and 5 min after NHB are less. Therefore, the therapeutic effect of the intervention could not be observed. For $NHB_{10\ min}$, the postoperative liver function significantly differed from that in the NHB_{0min} group. Moreover, the liver tissue necrosis increased significantly, and the 14-day survival rate was 16.7%. Consequently, we selected liver transplantation with 10 min of NHB as an ideal animal model for our subsequent experiments.

Characterization of MSCs-Exo and the protective effect of MSCs-Exo on NHB liver transplantation

The construction and identification of immortalized mouse MSCs are presented in Fig. 2, as reported in our previous study [6]. Then, we expanded and cultured the MSCs in vitro. MSCs-Exo were extracted and purified from the supernatant using the standard ultracentrifugation method at 110,000 g for 70 min twice. The nature and quality of the extracted exosomes were determined through transmission electron microscopy, which verified the vesicle structure and morphological characteristics

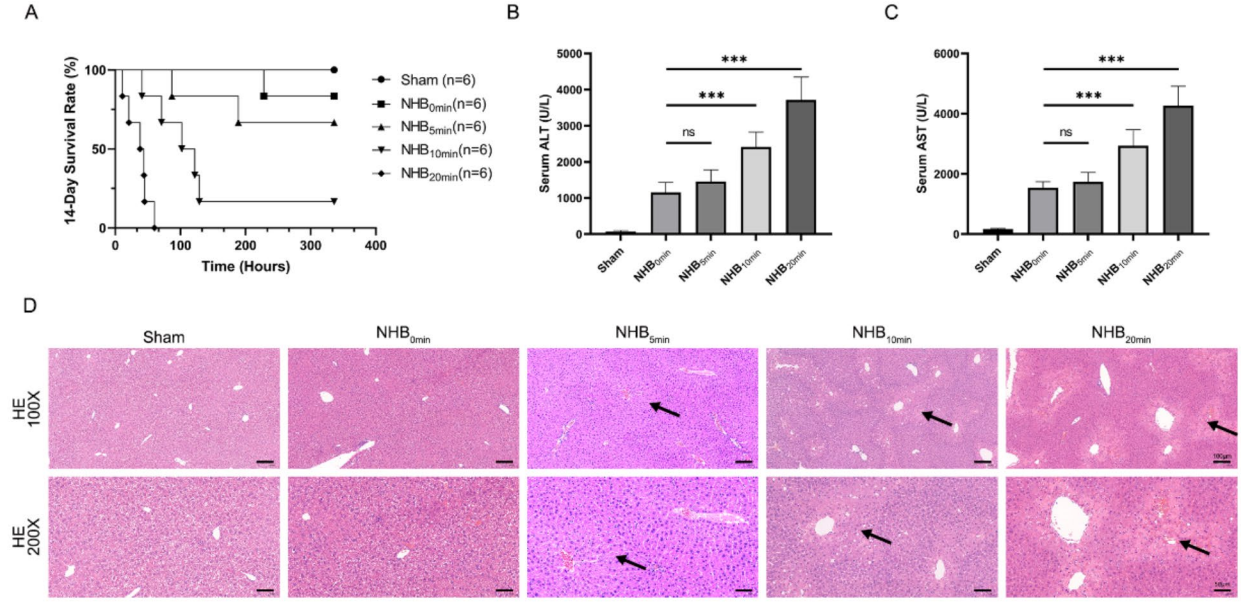

Fig. 1 Construction and validation of a mouse model of NHB liver transplantation. (**A**) The survival curves of mice from the sham and the NHB groups from 0 to 20 min. (**B**) and (**C**) Comparison of the changes in serum concentrations of ALT and AST 6 h post-transplantation among the sham and NHB groups time from 0 to 20 min. (**D**) Representative H&E staining images of liver tissues from the five groups of mice, 6 h post-transplantation. Black arrowheads indicate the necrosis areas. Magnification, 100×; scale bar, 100 μm and Magnification, 200×; scale bar, 50 μm

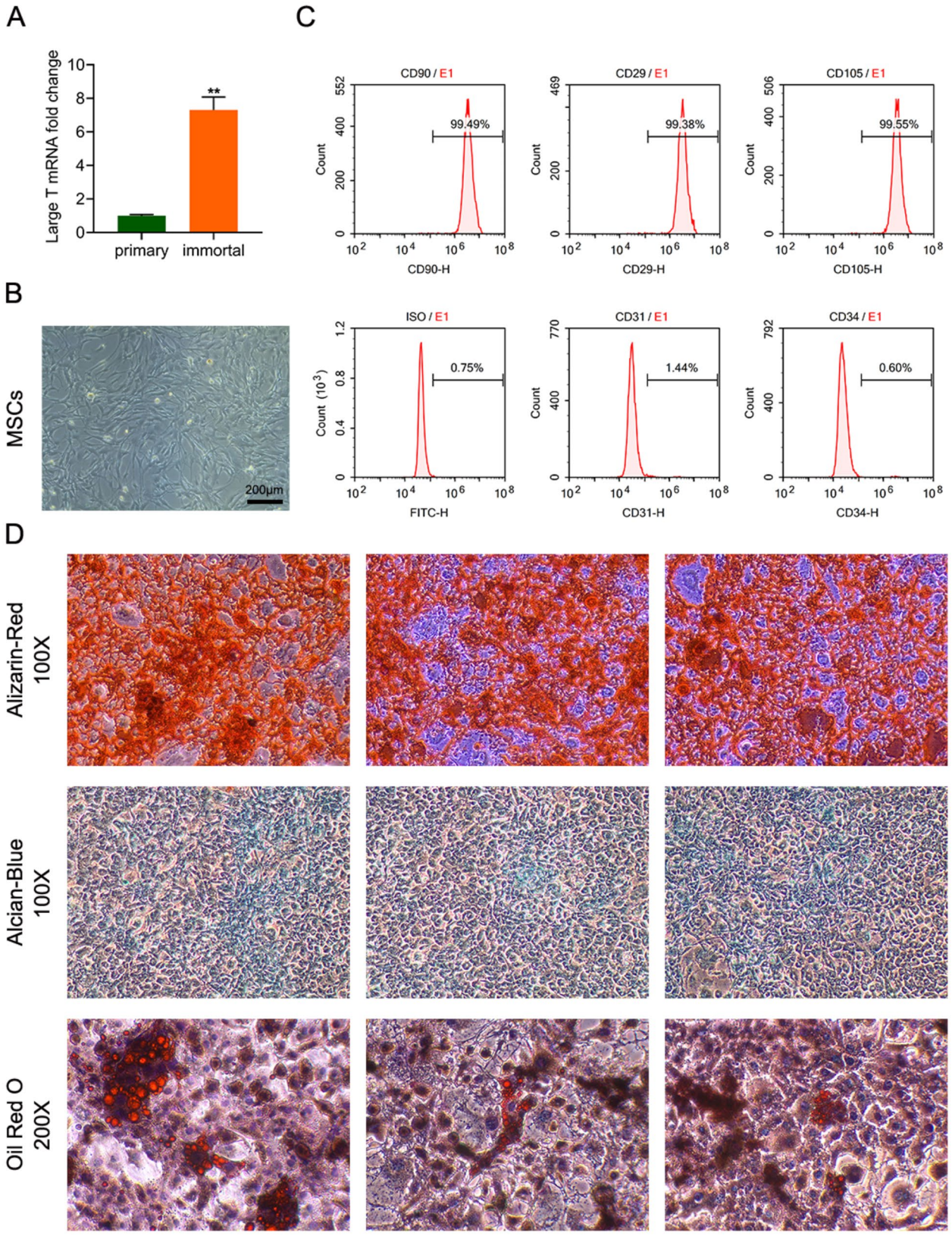

Fig. 2 Construction and identification of immortalized mouse MSCs. (**A**) Measurement of the mRNA levels of large T gene expression. (**B**) Representative images of the mouse bone marrow-derived mesenchymal stem cells (MSCs) under a light microscope. Scale bar, 200 μm. (**C**) Flow cytometry analysis of the expression of surface marker proteins of MSCs. (**D**) Representative staining images showing the osteogenic, chondrogenic and adipogenic differentiation of MSCs. Magnification, 100×; scale bar, 100 μm and Magnification, 200×; scale bar, 50 μm

of the MSCs-Exo (Fig. 3A). Additionally, nanoparticle tracking and western blotting analysis indicated that the diameter of MSCs-Exo was 78.2 ± 2.4 nm and the particles expressed CD81, HSP70, TSG101, CD63 and CD9, widely recognized as typical exosome molecular markers (Fig. 3B and C). Therefore, the MSCs-Exo were used to investigate the effect in NHB liver transplantation via injection of 250 μg of MSCs-Exo into the portal venous system 12 h in advance. We chose 250 μg because this dosage had a significant effect on postoperative survival rates and pyroptosis of Kupffer cells (Fig. 3D and E). As shown in Fig. 4A, the infusion of MSCs-Exo significantly increased the 14-day survival rate after 10 min of NHB from 0 to 66.7%. Furthermore, consistent with the results of the survival curve, liver function tests and HE staining suggested that MSCs-Exo exert a significant therapeutic effect in NHB liver transplantation (Fig. 4B-D). Compared with the NHB_{10min} group, the area of necrotic tissue and swollen degenerated cells around the portal area in the NHB_{10min} + MSCs-Exo group were significantly reduced. A group of blank injection was established to exclude the effects of PBS injection on survival rate (Fig. 4E), liver function tests (Fig. 4F and G), and HE staining following 10 min of NHB (Fig. 4H).

The infusion of MSCs-Exo significantly ameliorated NHB-induced graft injury and promoted the 14-day survival rate after NHB liver transplantation.

MSCs-Exo suppress pro-inflammatory cytokines and chemokine expression in liver grafts

Next, we evaluated the effect of MSCs-Exo on inflammatory cytokines and chemokine expression in the serum of recipients in both the control and experimental groups. Multiplex cytokine analysis was performed to measure the cytokines levels in mice serum. The results revealed that the infusion of MSCs-Exo effectively reduced the expression levels of pro-inflammatory cytokines, including IL-1β, IL-2, IL-4, IL-6, IL-16, TNF-α, IFN-γ, and MPO, and inflammatory chemokines, including CCL2, CCL3, CCL4, CCL7, CXCL1, and CXCL10. Moreover, it significantly increased the expression of the anti-inflammatory factor IL-10 (Fig. 5A and B). These findings suggested that MSCs-Exo effectively downregulate the expression of pro-inflammatory factors, including IL-1β and TNF-α, and pro-inflammatory chemokines, including CXCL1, in the liver after transplantation. Additionally, MSCs-Exo increased the expression of anti-inflammatory factors, including IL-10, thereby reducing the postoperative liver function damage.

Kupffer cells: the key to the efficacy of MSCs-Exo therapy

Kupffer cells in the liver are crucial sensor cells that initiate damage signals and mediate immune responses. They are vital in regulating the liver's natural immunity, countering danger signals, and maintaining liver immune homeostasis. Moreover, our previous studies on MSCs have highlighted the potential importance of Kupffer cells [6]. To determine whether Kupffer cells are the key cells for the protective effect of MSCs-Exo, we used an intraperitoneal injection of $GdCl_3$ to systematically deplete Kupffer cells in the donor liver. The survival rate of the NHB_{10min} + $GdCl_3$ group after liver transplantation exhibited no improvement compared to the NHB_{10min} group. Moreover, even with the infusion of MSCs-Exo post-transplantation, the postoperative survival rate of the NHB_{10min} + $GdCl_3$ + MSCs-Exo group was not significantly different from that of the NHB_{10min} group (Fig. 6A). Additionally, as shown in Fig. 6B and C, after the elimination of intrahepatic Kupffer cells, postoperative liver function markers ALT and AST exhibited a slight increase with no significant difference. The infusion of MSCs-Exo could not effectively improve postoperative liver function. The results of pathological HE staining of the transplanted liver tissue were consistent with the liver function assay (Fig. 6D). Then, F4/80, a macrophage surface marker, was used to detect the number and distribution of Kupffer cells in the liver. As shown in Fig. 6E, immunofluorescence results indicated that early infusion of $GdCl_3$ resulted in almost no F4/80-positive Kupffer cells, supporting the notion that $GdCl_3$ effectively eliminates Kupffer cells in the liver. The infusion of MSCs-Exo restored the quantity and vitality of F4/80-positive Kupffer cells. However, when $GdCl_3$ was used in advance, even MSCs-Exo could not reverse the depletion of F4/80-positive Kupffer cells. In summary, when the Kupffer cells in the transplanted liver were depleted, MSCs-Exo lost its protective effect on liver transplantation. This suggests that Kupffer cells play a key role in mediating the efficacy of MSCs-Exo therapy.

MSCs-Exo effectively reduce pyroptosis of Kupffer cells in liver grafts

Multiple studies suggest that Kupffer cells could sense damage signals and regulate the expression of inflammatory factors and chemokines through the classical pyroptosis pathway through Caspase1 expression [32, 33]. This process increases inflammation, hepatic damage, and necrosis [34]. Our results suggested that multiple inflammatory factors are released after transplantation, and MSCs-Exo can effectively alleviate the progression of inflammation. Therefore, we hypothesized that MSCs-Exo could reduce graft damage by inhibiting pyroptosis. Furthermore, Caspase1, a classic pyroptosis surface marker, was used to detect pyroptosis of Kupffer cells in different groups (Fig. 7A). The results suggested that the infusion of MSCs-Exo reduced pyroptosis of Kupffer cells in the transplanted liver. This action thereby reduced a series of inflammatory reactions and exerted a

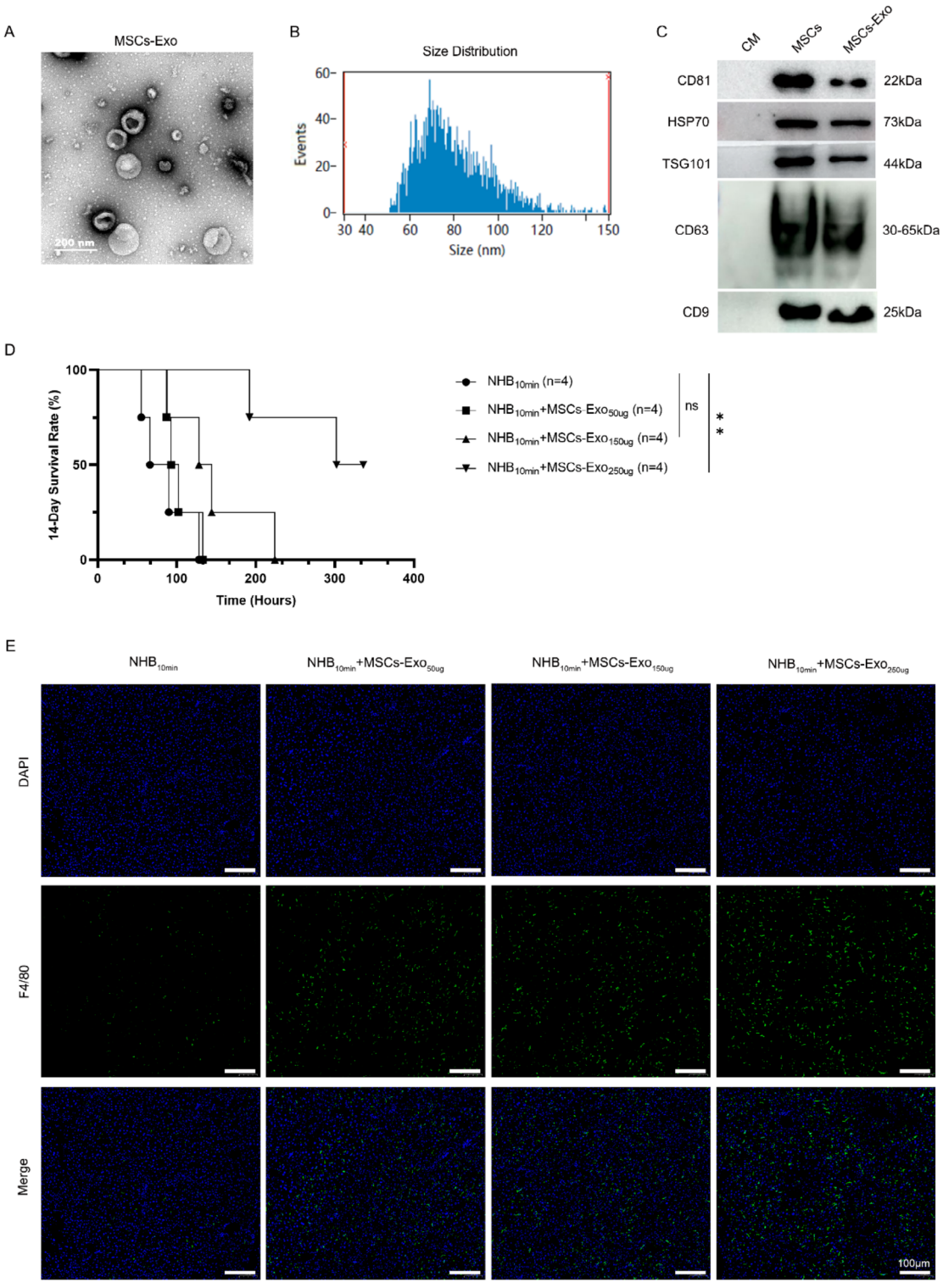

Fig. 3 Characterization of MSCs-Exo and comparative analysis of the protective effects at different doses. (**A**) Representative transmission electron microscopy images of the MSCs-Exo. Scale bar, 200 nm. (**B**) Measurement of the protein levels of CD81, HSP70, TSG101, CD63 and CD9 in the conditioned medium (CM), MSCs, and MSCs-Exo groups. (**C**) The nanoparticle tracking analysis of the MSCs-Exo. (**D**) The survival curves of the NHB_{10min} group, NHB_{10min} + MSCs-$Exo_{50\mu g}$ group, NHB_{10min} + MSCs-$Exo_{150\mu g}$ group and NHB_{10min} + MSCs-$Exo_{250\mu g}$ group 14 days post-transplantation. (**E**) Representative immunofluorescence staining of F4/80 (green) in liver tissues from the indicated groups, 6 h post-transplantation. Scale bar, 100 μm

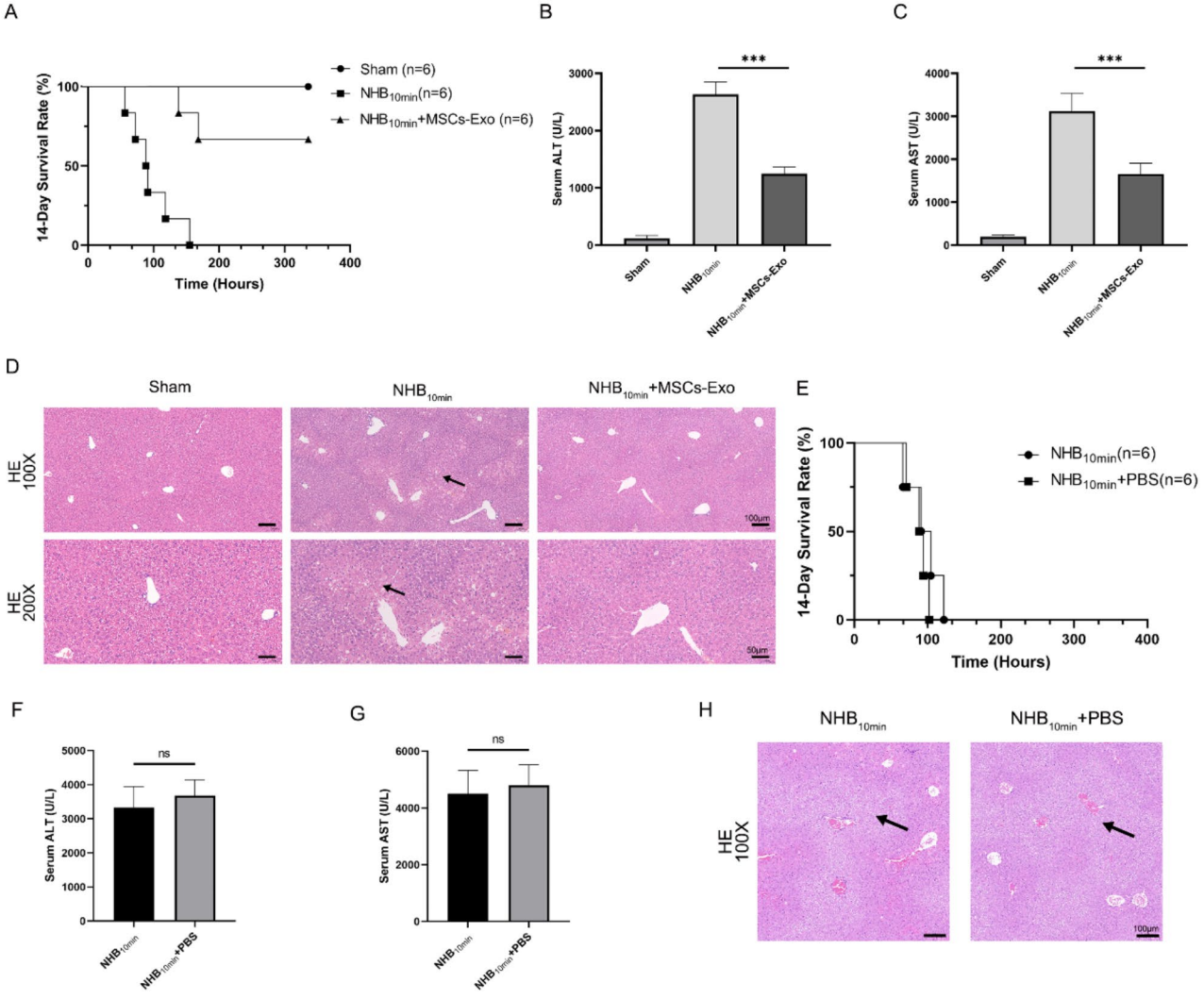

Fig. 4 The protective effect of MSCs-Exo on NHB liver transplantation. (**A**) The survival curves for mice from the sham group, NHB_{10min} group and NHB_{10min} + MSCs-Exo group 14 days post-transplantation. (**B**) and (**C**) Analysis of the concentration of serum ALT and AST 6 h post-transplantation among the sham group, NHB_{10min} group and NHB_{10min} + MSCs-Exo group. (**D**) Representative H&E staining images of mice liver tissues from the three groups, 6 h post-transplantation. Black arrowheads indicate necrosis areas. Magnification, 100×; scale bar, 100 μm and Magnification, 200×; scale bar, 50 μm. (**E**) The survival curves of the NHB_{10min} group and NHB_{10min} + PBS group 14 days post-transplantation. (**F**) and (**G**) Comparison of the serum concentration of ALT and AST 6 h post-transplantation between the NHB_{10min} group and NHB_{10min} + PBS group. (**H**) Representative H&E staining images of mice liver tissues from the two groups. Black arrowheads indicate necrosis areas. Scale bar, 100 μm

protective effect on the liver function and liver damage in the transplanted liver by Kupffer cell pyroptosis. Then, the mouse-derived macrophage cell line RAW 264.7 was used to mimic the replacement of Kupffer cells in vivo. Under in vitro co-culture conditions, 300 μM H_2O_2 was used to simulate ischemia-reperfusion injury caused by liver transplantation. The results revealed that MSCs-Exo effectively inhibited the gene expression of pro-inflammatory cytokines, including IL-1β, IL-2, IL-6, IL-18, TNF-α, and IFN-γ (Fig. 7B). To enhance our understanding of the interaction between MSCs-Exo and Kupffer cells, DiI (red)-labeled MSCs-Exo were introduced to cultured RAW 264.7 cells. Following a 6-hour incubation period, the MSCs-Exo were internalized by the RAW 264.7 cells and subsequently localized in the cytoplasm (Fig. 7C). These data indicated that MSCs-Exo effectively reduced pyroptosis of Kupffer cells in liver grafts.

Mir-17-5p as a candidate effector of MSCs-Exo mediated pyroptosis of Kupffer cells

We performed miRNA sequencing screening to investigate the mechanism of MSCs-Exo-mediated pyroptosis in Kupffer cells. Subsequently, PCR assays validated the expression of common miRNAs associated with

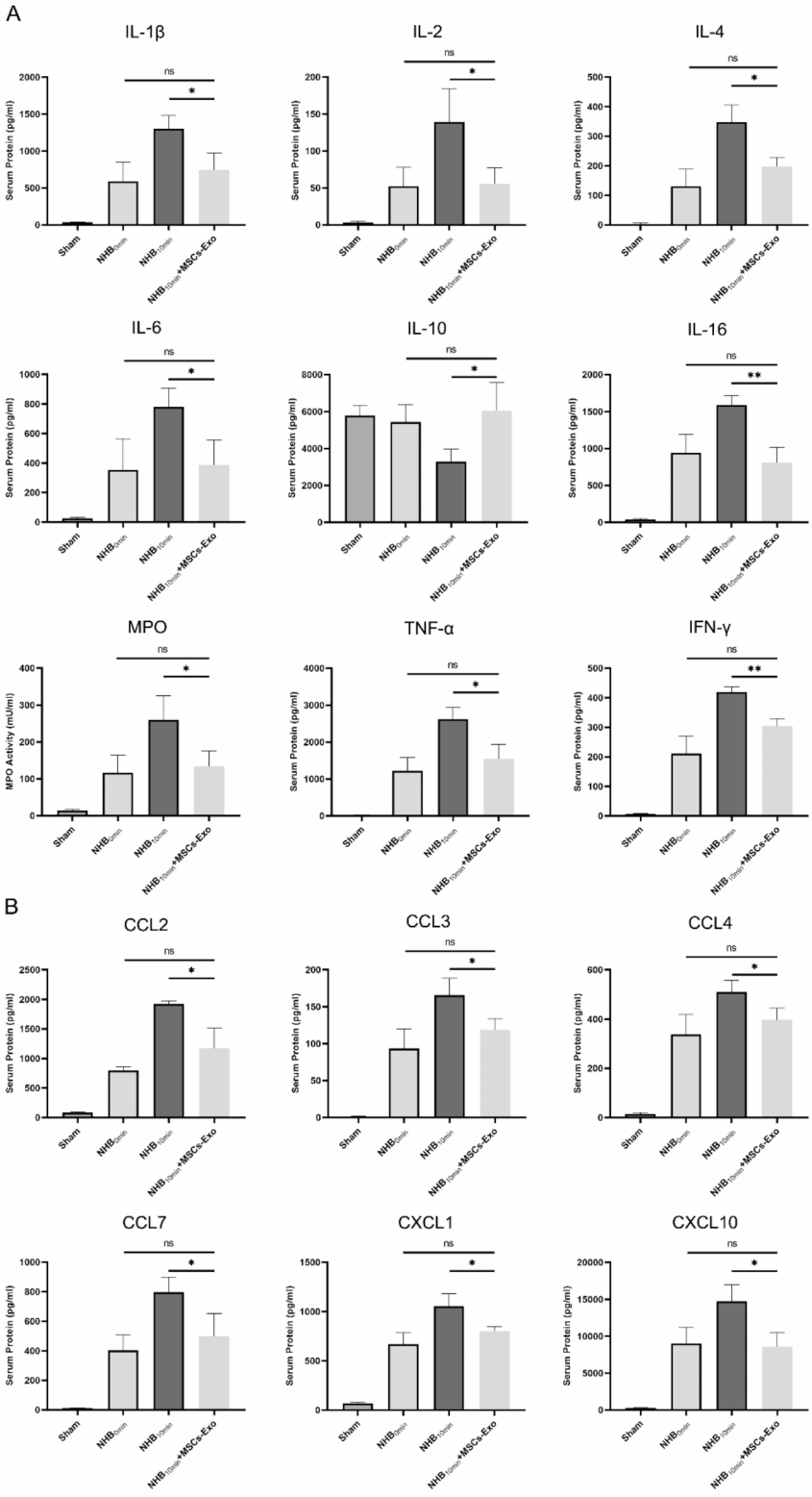

Fig. 5 MSCs-Exo suppressed pro-inflammatory cytokines and chemokine secretion in liver grafts. Quantification of the protein expression of (**A**) pro-inflammatory cytokines and (**B**) chemokines in the serum from the Sham group, NHB_{0min} group, NHB_{10min} group and NHB_{10min}+MSCs-Exo group 6 h post-transplantation

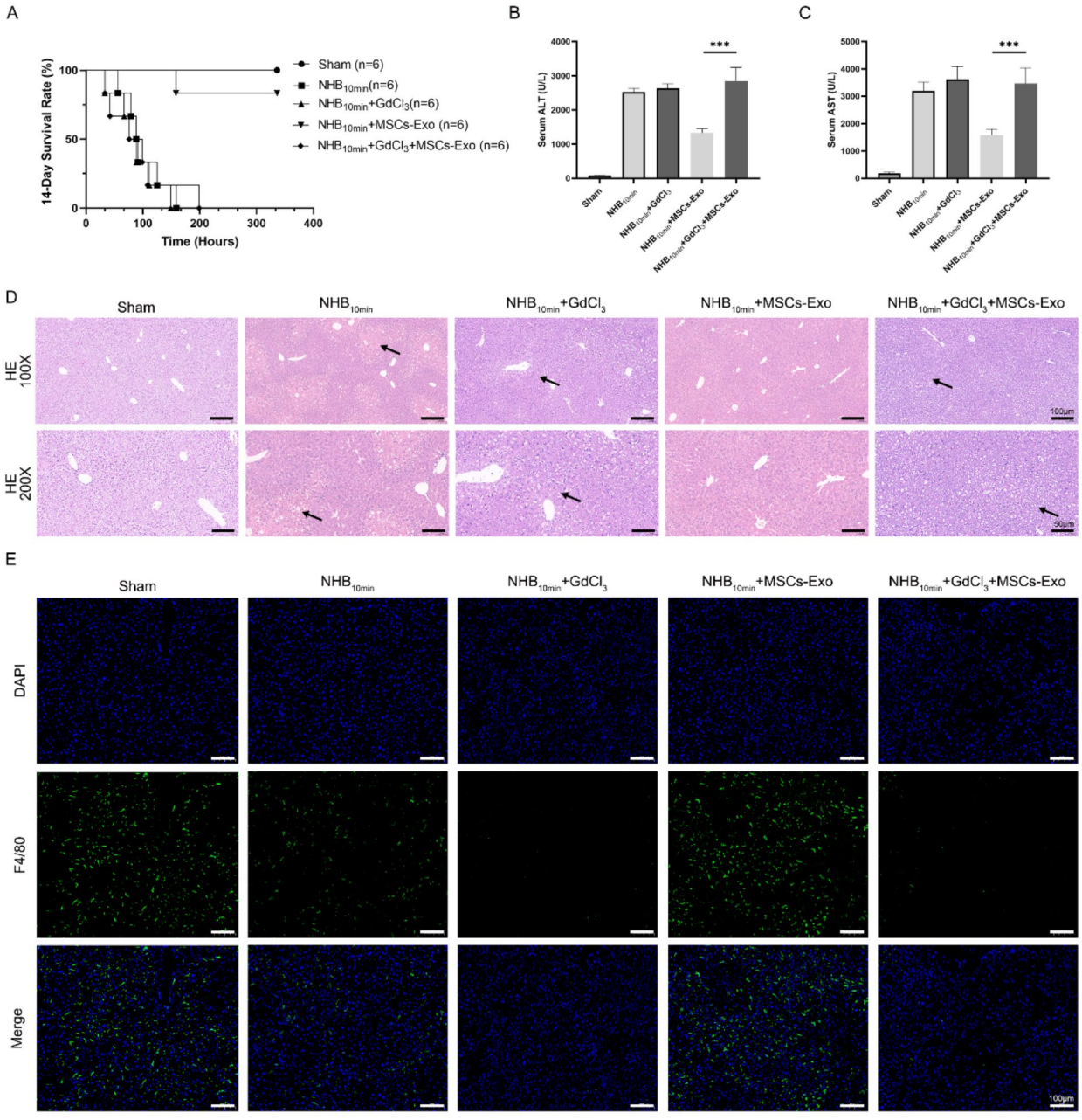

Fig. 6 Kupffer cells mediated the efficacy of MSCs-Exo therapy. (**A**) Survival curves of the Sham group, NHB_{10min} group, $NHB_{10min}+GdCl_3$ group, NHB_{10min}+MSCs-Exo group and $NHB_{10min}+GdCl_3$+MSCs-Exo group 14 days post-transplantation. (**B**) and (**C**) Comparison of serum concentrations of ALT and AST 6 h post-transplantation among the five groups of mice. (**D**) Representative H&E staining images of mice liver tissues from the five groups, 6 h post-transplantation. Black arrowheads indicate necrosis areas. Magnification, 100×; scale bar, 100 μm and Magnification, 200×; scale bar, 50 μm. (**E**) Representative immunofluorescence staining images of F4/80 (green) in the liver tissues in the indicated groups, 6 h post-transplantation. Scale bar, 100 μm

pyroptosis. As described previously, the relatively stable miR-16-5p expression was used as the baseline control [35]. The results suggested that miR-17-5p expression in MSCs-Exo was abundant and relatively the highest (Fig. 8A). As a result, we hypothesized that MSCs-Exo exerted a series of regulatory and cytoprotective effects through miR-17-5p. Subsequently, MSC cell lines with low miR-17-5p expression were transfected with lentivirus, while MSC cell lines containing control was also established. The miR-17-5p expression levels in the

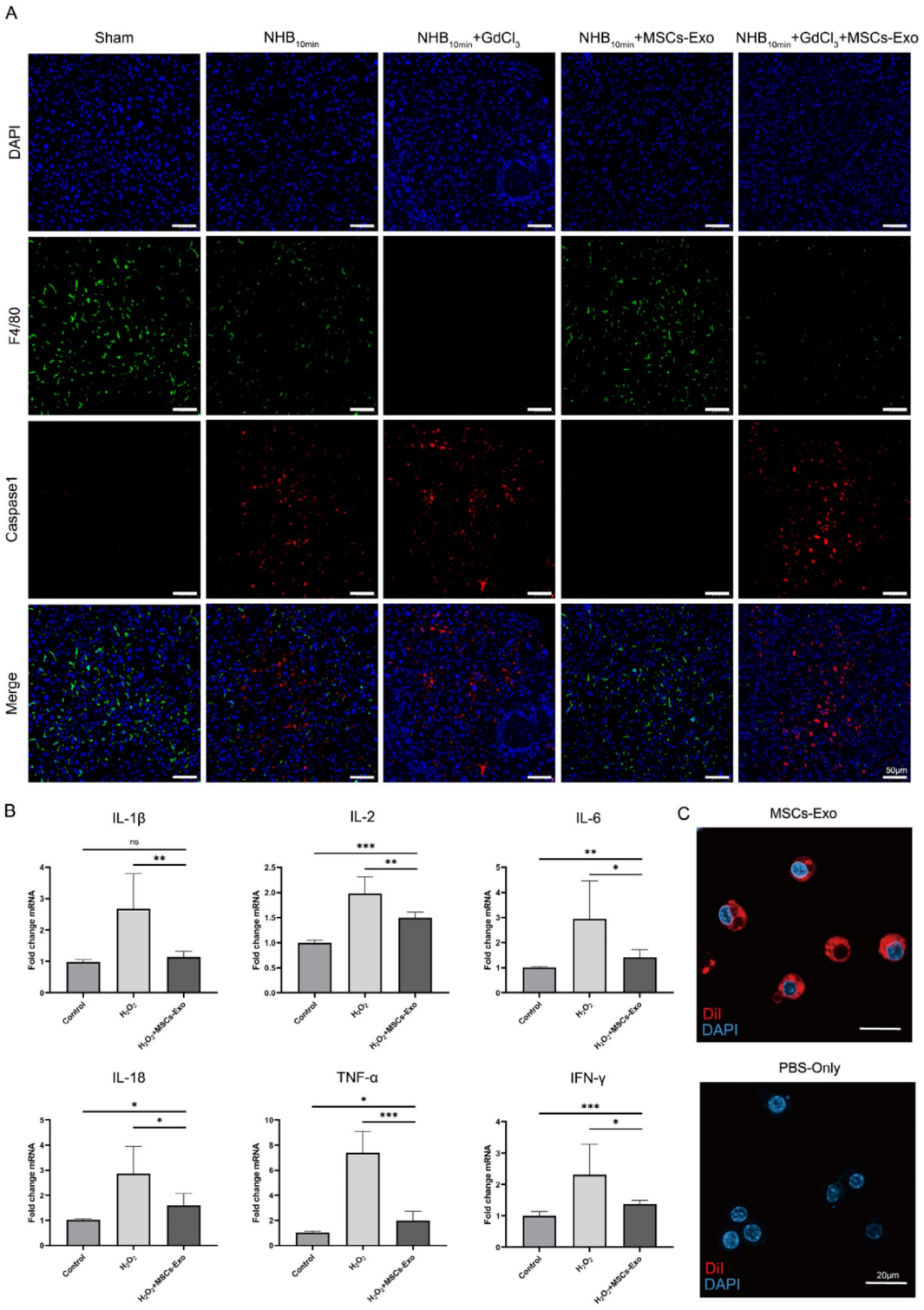

Fig. 7 MSCs-Exo effectively reduced pyroptosis of Kupffer cells in liver grafts. (**A**) Representative immunofluorescence staining of F4/80 (green) and Caspase1 (red) in the Sham group, NHB_{10min} group, $NHB_{10min}+GdCl_3$ group, $NHB_{10min}+$MSCs-Exo group and $NHB_{10min}+GdCl_3+$MSCs-Exo group, 6 h post-transplantation. Scale bar, 50 μm. (**B**) Comparison of the gene expression of IL-1β, IL-2, IL-6, IL-18, TNF-α, IFN-γ. The mRNA levels of these genes were normalized to the expression of β-actin gene and presented as fold change. (**C**) Representative images depicting the uptake of DiI-labeled MSCs-Exo (red) by RAW 264.7 cells (DAPI blue), and comparison of the fluorescence uptake with PBS-only controls. The PBS-only group showing the basal fluorescence of RAW264.7 cells. Scale bar, 20 μm

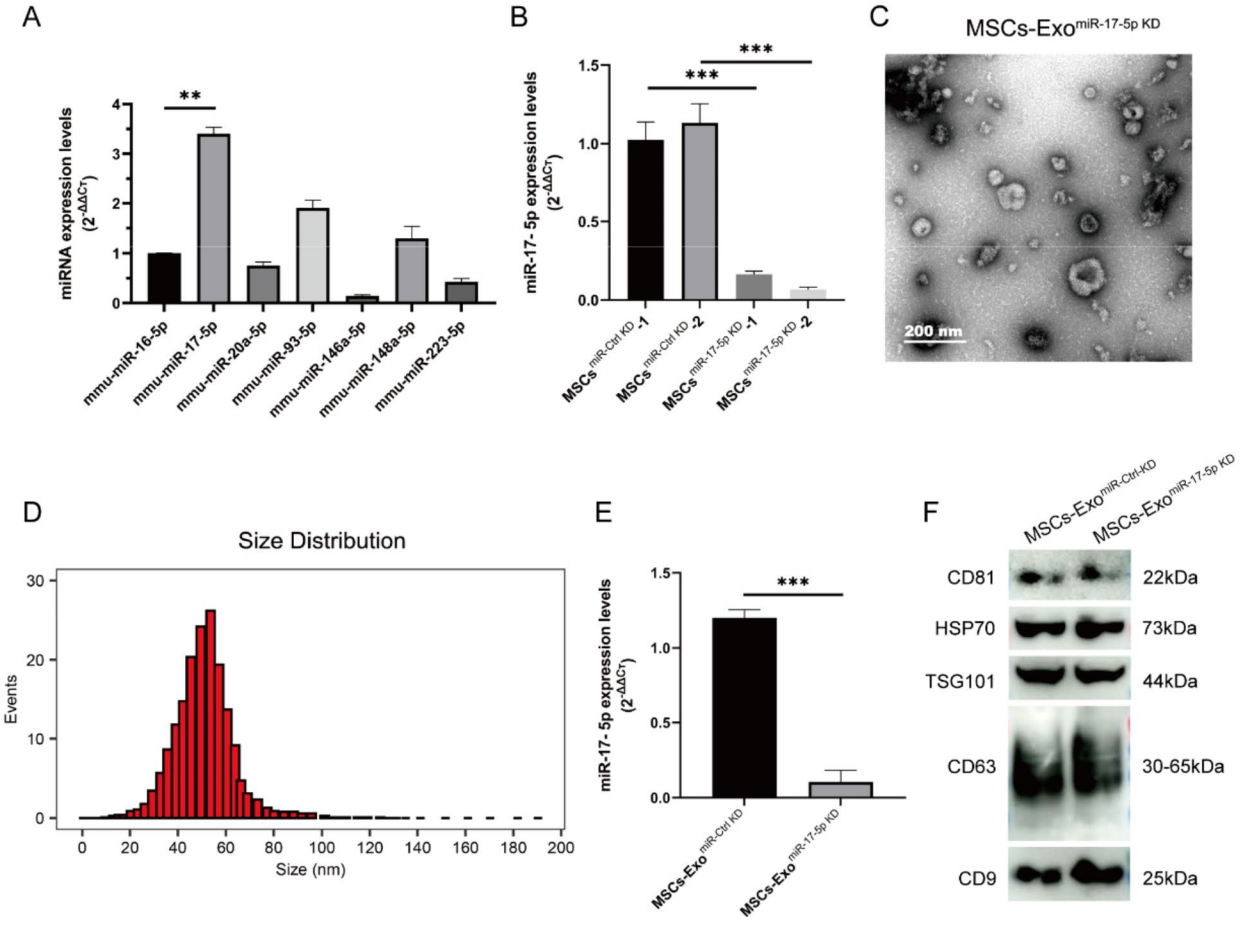

Fig. 8 Construction and characterization of MSCs-Exo with knock down of miR-17-5p. (**A**) The relative expression level of several pyroptosis-related miRNA genes in MSCs-Exo. The miRNA expression was normalized to that of miR-16-5p. (**B**) Comparison of miR-17-5p expression levels in MSC cells after transfection with lentiviral-shRNA and lentivirus-control. (**C**) Representative transmission electron microscopy images of exosomes extracted from MSC cells transfected with the lentiviral-shRNA-miRNA-17-5p. (**D**) The nanoparticle tracking analysis of the MSCs-Exo$^{miR-17-5p\ KD}$. (**E**) Comparison of miR-17-5p expression levels between the MSCs-Exo$^{miR-Ctrl-KD}$ and MSCs-Exo$^{miR-17-5p\ KD}$ groups. (**F**) The protein levels of CD81, HSP70, TSG101, CD63 and CD9 were measured in the MSCs-Exo$^{miR-Ctrl-KD}$ group and MSCs-Exo$^{miR-17-5p\ KD}$ group

lentivirus-transfected MSC cell lines and the exosomes extracted from the two transfected cells were determined (Fig. 8B-E). The diameter of MSCs-Exo$^{miR-17-5p\ KD}$ was 58.8 ± 6.8 nm. Western blotting analysis indicated that proteins CD81, HSP70, TSG101, CD63, and CD9 were also detectably expressed in the MSCs-Exo$^{miR-17-5p\ KD}$ group (Fig. 8F).

Next, we used these two types of exosomes with different miR-17-5p levels to investigate their protective effects in the in vivo mouse liver transplant model. As shown in the Fig. 9A, the 14-day postoperative survival rate of transplant mice infused with MSCs-Exo$^{miR-Ctrl-KD}$ was similar to that of infusion with normal MSCs-Exo. However, those infused with MSCs-Exo$^{miR-17-5p\ KD}$ exhibited a significantly decreased 14-day postoperative survival rate (Fig. 9A). Consistent with the survival curve results, liver function and HE staining analyses in the MSCs-Exo$^{miR-17-5p\ KD}$ group were not significantly different compared to the NHB_{10min} group (Fig. 9B-D). The transplanted livers infused with MSCs-Exo$^{miR-17-5p\ KD}$ exhibited similar patchy hepatic parenchymal necrosis around the portal area as observed in the NHB_{10min} group. However, the extent of liver parenchymal necrosis and liver cell degeneration was significantly reduced in the MSCs-Exo$^{miR-Ctrl-KD}$ group. Additionally, to demonstrate that miR-17-5p can reduce Kupffer cell-mediated activation of neutrophils and T cells, immunohistochemistry staining of CD3 and MPO was performed in the NHB_{10min} group, NHB_{10min} + MSCs-Exo$^{miR-Ctrl-KD}$ group, and NHB_{10min} + MSCs-Exo$^{miR-17-5p\ KD}$ group (Fig. 9E). Compared to the NHB_{10min} group, the addition of MSCs-Exo$^{miR-Ctrl-KD}$ resulted in a significant decrease in both neutrophils and T cells. However, in the NHB_{10min} + MSCs-Exo$^{miR-17-5p\ KD}$ group, the immunohistochemical staining was not significantly different compared to the NHB_{10min} group. This suggests that

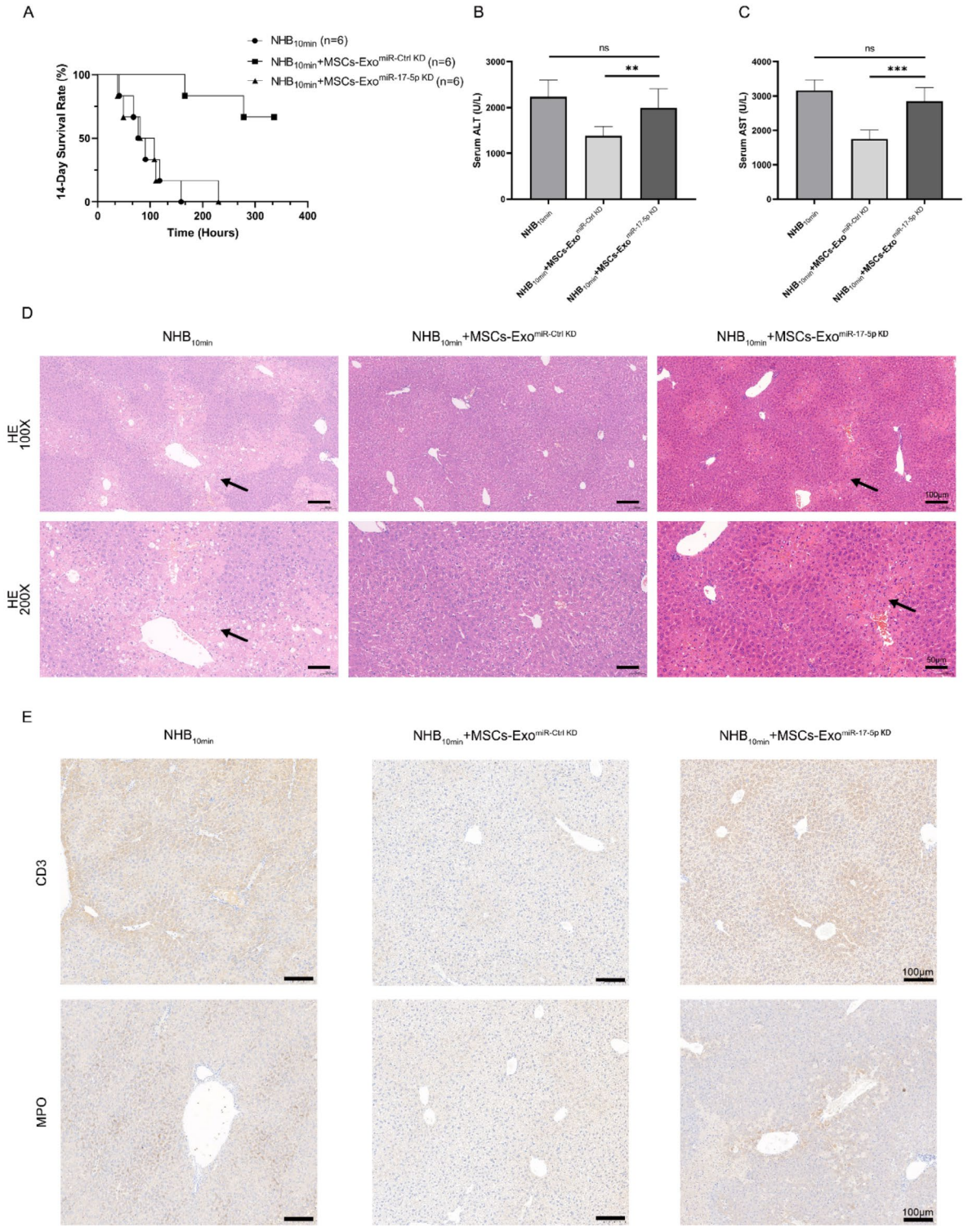

Fig. 9 miR-17-5p, a candidate effector in MSCs-Exo, mediated the pyroptosis of Kupffer cells. (**A**) Survival curves of the NHB_{10min} group, NHB_{10min} + MSCs-$Exo^{miR-Ctrl-KD}$ and NHB_{10min} + MSCs-$Exo^{miR-17-5p\ KD}$ group 14 days after transplantation. (**B**) and (**C**) Comparison of serum concentration of ALT and AST 6 h post-transplantation among the three groups of mice. (**D**) Representative H&E staining images of mice liver tissues from the three groups 6 h post-transplantation. Black arrowheads indicate necrosis areas. Magnification, 100×; scale bar, 100 μm and Magnification, 200×; scale bar, 50 μm. (**E**) Representative immunohistochemistry staining images of CD3 (brown) and MPO (brown) in the NHB_{10min} group, NHB_{10min} + MSCs-$Exo^{miR-Ctrl-KD}$ group and NHB_{10min} + MSCs-$Exo^{miR-17-5p\ KD}$ group, 6 h post-transplantation. Scale bar, 100 μm

without or with low miR-17-5p expression in MSCs-Exo, its protective effect on the liver grafts is eliminated.

Mir-17-5p shuttling by MSCs-Exo inhibits Kupffer cell pyroptosis by regulating the TXNIP-NLRP3-Caspase1 signaling pathway

To further investigate the underlying mechanism by which MSCs-Exo protects Kupffer cells and reduces pyroptosis, we focused on the target gene of miR-17-5p within macrophages. Previous studies indicate that miR-17-5p can regulate TXNIP protein expression, agitate the NLRP3 inflammasome, and subsequently trigger classic pyroptosis's Caspase1 cell signaling pathway [36, 37]. To explore this hypothesis, we utilized an in vitro cell–cell co-culture system with the RAW264.7 cell line to represent Kupffer cells. Following H_2O_2 stimulation for 24 h, the activated TXNIP protein expression was significantly higher than the controls. However, co-culture with MSCs-Exo$^{miR-Ctrl-KD}$ effectively reduced TXNIP protein expression. Moreover, the inhibitory effect on the TXNIP protein was significantly reversed in the presence of MSCs-Exo$^{miR-17-5p\ KD}$ (Fig. 10A). Subsequently, we investigated the downstream classic pyroptosis pathway mediated by TXNIP. Oxidative stress damage induced by H_2O_2 promoted the TXNIP protein expression in Kupffer cells, which activated the NLRP3 inflammasome, thereby resulting in the cleavage and activation of Caspase1. Treatment with MSCs-Exo$^{miR-Ctrl-KD}$ effectively reduced the TXNIP protein expression, thereby inhibiting NLRP3 inflammation activation and the classic pyroptosis pathway. However, the inhibitory effect of the MSCs-Exo$^{miR-17-5p\ KD}$ group on TXNIP, NLRP3, and Caspase1 protein expression was significantly reduced (Fig. 10B). As shown in the Fig. 10C, as a positive control group, H_2O_2 induced the activation and expression of TNXIP protein in normal Kupffer cells, activating downstream NLRP3 protein and Caspase1 protein. Overexpression with TXNIP and H_2O_2 stimulation resulted in higher TXNIP protein expression. The infusion of MSCs-Exo$^{miR-Ctrl-KD}$ moderately inhibited the TXNIP protein expression in the Kupffer cell, which was transfected with the TXNIP overexpression plasmid. However, compared with the H_2O_2 + OE-TXNIP group, MSCs-Exo$^{miR-17-5p\ KD}$ did not significantly affect the TXNIP protein expression level, promoting pyrolysis in Kupffer cells. Furthermore, the transcriptional regulation of miR-17-5p on the TXNIP promoter was detected by luciferase reporter assays (Fig. 11A). The results showed that expression of miR-17-5p has significant effect on the promoter transcription of TXNIP in 293T cells transfected with wild type promoter of TXNIP luciferase reporter vectors but no effect on the mutant promoter of TXNIP luciferase reporter vectors. Thus, our results indicating that miR-17-5p can regulate the expression of its downstream TXNIP, thereby regulating the progression of inflammation. The mechanistic presentation of this study has been described in Fig. 11B. In summary, our results confirmed the critical role of miR-17-5p in inhibiting Kupffer cell pyroptosis through the TXNIP-NLRP3-Caspase1 signaling pathway.

Discussion

Liver transplantation is the optimal effective treatment for end-stage liver disease. However, the shortage of donor livers has become a serious problem restricting the development of liver transplantation [38]. DCD donors have become an important strategy to increase the source of liver donors. However, due to the inevitable ischemia-reperfusion injury during DCD donation, the incidence of short-term graft loss and long-term biliary complications after DCD liver transplantation increases significantly [6, 39]. Our preliminary research indicates that the infusion of MSCs can effectively inhibit the decrease in the number of F4/80 + Kupffer cells in transplanted donor livers. This results in reduced damage and inflammatory response of DCD donor livers in mice, significantly improving the survival rate in recipient mice after transplantation. Furthermore, MSCs and Kupffer cells were co-cultured in vitro using a transwell system. The results revealed that even without direct contact with cells, MSCs still effectively mitigate Kupffer cell damage induced by high concentrations of oxidative stress damage through paracrine effects. This suggests the presence of a mediator that mediates the protective effects of MSCs [6]. Based on the literature search, we hypothesize that MSCs-Exo are the primary mediators.

Intrahepatic Kupffer cell pyroptosis is the primary cause of warm ischemia/reperfusion injury in DCD donor livers; therefore, we performed immunofluorescence staining on donor liver tissue specimens to investigate the impact of MSCs-Exo on Kupffer cell pyroptosis. The results revealed a decrease in the number of F4/80 and caspase1 double-positive Kupffer cells in the donor liver. Furthermore, the NLRP3 protein expression levels and caspase1 associated with the classic pyroptotic pathway in Kupffer cells were significantly decreased. Accordingly, we hypothesized that MSCs-Exo can protect DCD donor livers by inhibiting Kupffer cell pyroptosis through the classic NLRP3 and Caspase1 pathway.

MSCs-Exo contain more than 150 miRNAs, and their abundant miRNAs can exert directional regulatory effects on target genes [40]. We investigated the potential mechanism by which MSCs-Exo reduces the expression of proteins, including NLRP3 and Caspase1, and inhibit Kupffer cell pyroptosis. We identified several miRNA families potentially associated with the classical cell pyroptosis pathway through exosome miRNA sequencing and a literature search. Through RT-PCR

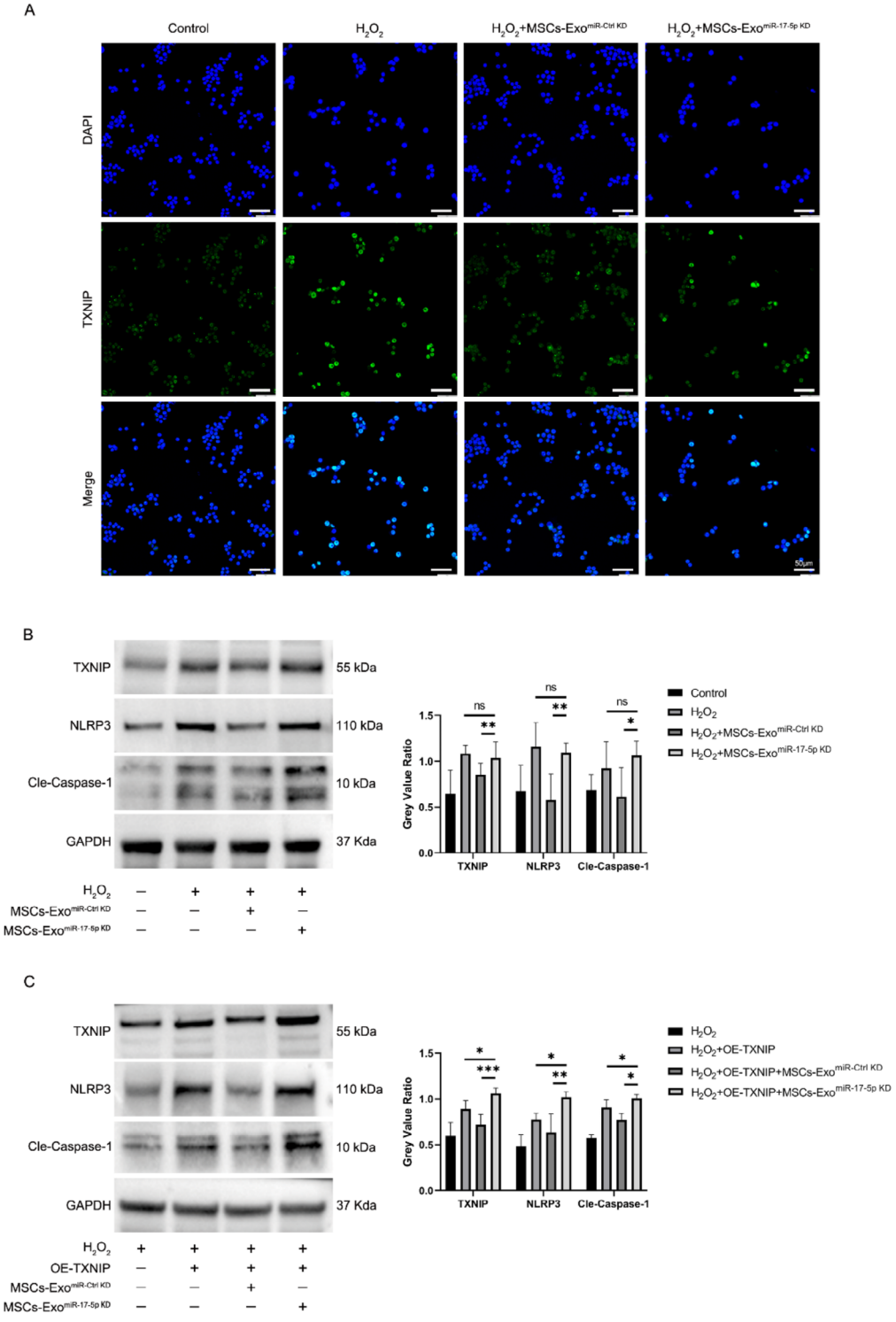

Fig. 10 miR-17-5p shuttling by MSCs-Exo inhibited Kupffer cell pyroptosis by regulating the TXNIP-NLRP3-Caspase1 signaling pathway. (**A**) Representative immunofluorescence staining images of TXNIP (green) in Kupffer cells treated with MSCs-Exo$^{miR-Ctrl-KD}$ and MSCs-Exo$^{miR-17-5p\ KD}$ under 300μM H_2O_2 stimulation. (**B**) Comparison of the protein levels of TXNIP, NLRP3 and Cle-caspase1 in the Control, H_2O_2, H_2O_2 + MSCs-Exo$^{miR-Ctrl-KD}$ and H_2O_2 + MSCs-Exo$^{miR-17-5p\ KD}$ groups. (**C**) The TXNIP protein was overexpressed in the OE-TXNIP Kupffer cells. The protein levels of TXNIP, NLRP3 and Cle-caspase1 were measured in the H_2O_2, H_2O_2 + OE-TXNIP, H_2O_2 + OE-TXNIP + MSCs-Exo$^{miR-Ctrl-KD}$ and H_2O_2 + OE-TXNIP + MSCs-Exo$^{miR-17-5p\ KD}$ groups

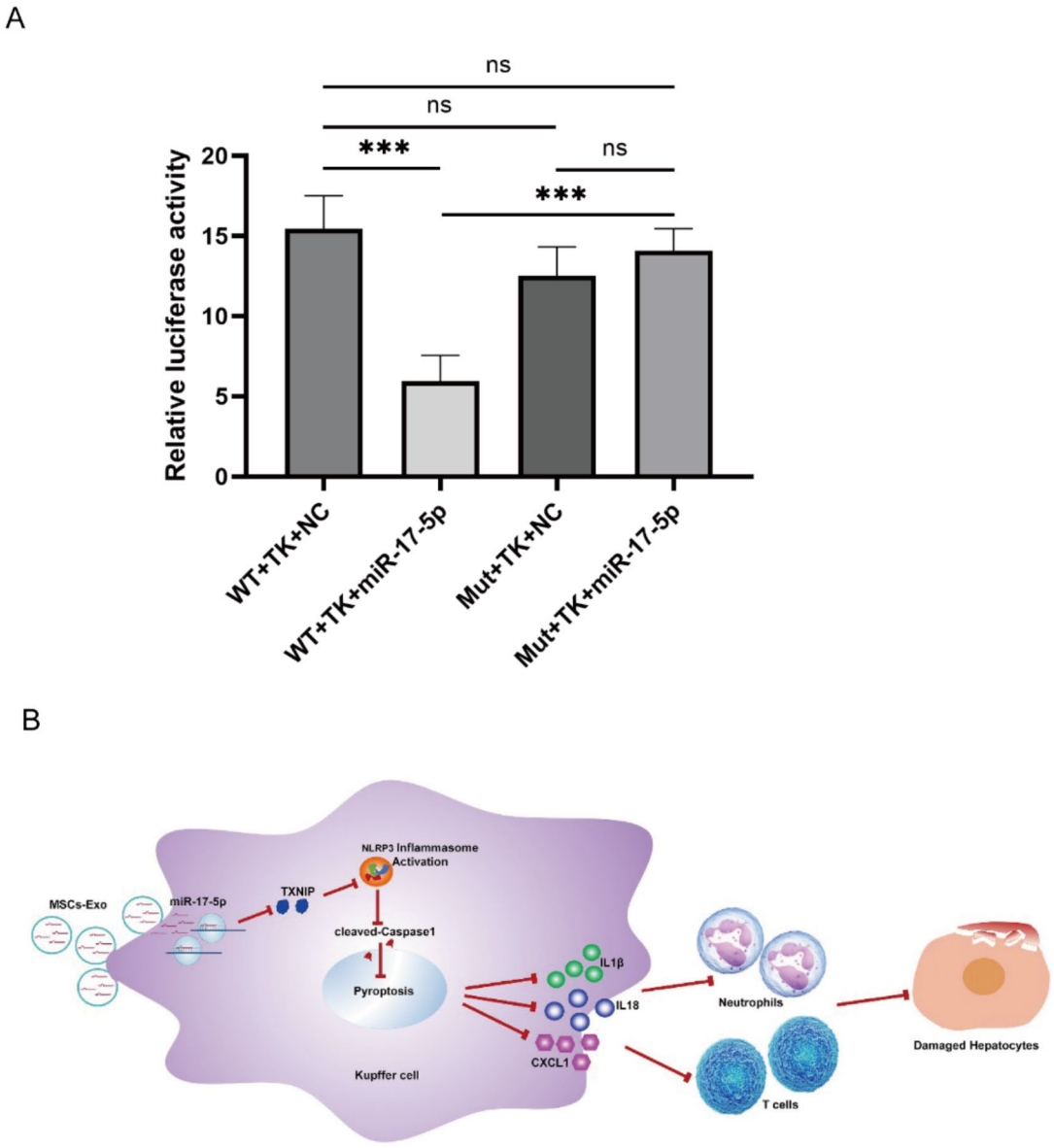

Fig. 11 Results of the luciferase reporter assays and the mechanism diagram for this study. (**A**) The transcriptional regulatory mechanism of miR-17-5p on the TXNIP promoter was determined by the luciferase reporter assays. (**B**) The mechanism diagram of this research

re-validation of miRNAs, we found that miRNA-17-5p had the highest content, suggesting that MSCs-Exo can inhibit Kupffer cell pyroptosis of the classical pathway through high miRNA-17-5p expression. Moreover, we found that the TXNIP expression can be negatively regulated by miRNA-17-5p. Previous research has reported that TXNIP could bind to NLRP3 in metabolic and myocardial ischemic diseases, activating the NLRP3 inflammasome and further agitating the classical pyroptosis signaling pathway [11]. Therefore, we determined that miRNA-17-5p could target the TXNIP expression, inhibiting the classical Kupffer cell pyroptosis pathway.

There are certain limitations in this study. We only performed the miRNA-17-5p knockdown and TXNIP overexpression. We did not fully execute the miRNA-17-5p overexpression and the TXNIP knockdown, which affected the integrity of our study to a certain extent. Additionally, we only performed animal experiments to investigate the protective effect of MSCs-Exo on liver transplantation donors. Consequently, further studies on human liver transplantation are required for clinical application. Furthermore, in the animal experiments conducted for this study, some of the macrophages presented in the mouse liver might originate from the recipient's bone marrow or spleen, a detail that was not explicitly

elucidated in our current research. In subsequent studies, we aim to provide a clearer understanding of the donor-specific Kupffer cells as well as the recipient-derived macrophages within the donor liver. Finally, macrophage polarization into M1 and M2 phenotypes is associated with distinct functions and effects. We hypothesize that during the ischemia-reperfusion injury phase in liver transplantation, there was a shift in macrophage polarization. However, due to time and budget constraints, this paper does not delve deeply into this aspect. Future studies will focus on elucidating the differential M1/M2 polarization in macrophages, specifically Kupffer cells.

Notably, the underlying mechanism revealed in our research broadens insight and provides a solid theoretical foundation for a better understanding of how MSCs-Exo protect NHB grafts, offering new treatment strategies for alleviating the problem of organ shortage.

Conclusions

In conclusion, we investigated the therapeutic potential of MSCs-Exo in liver transplantation, particularly focusing on their impact on Kupffer cell pyroptosis. Our findings demonstrate that MSCs-Exo significantly reduced the expression of pro-inflammatory cytokines and chemokines while enhancing anti-inflammatory factors. This decreased necroptosis in liver grafts, improving postoperative liver function and survival rates. Mechanistically, MSCs-Exo exert their protective effects through miR-17-5p, which targets the TXNIP-NLRP3-Caspase1 signaling pathway, thereby inhibiting Kupffer cell pyroptosis. Our research highlights the pivotal role of miR-17-5p in MSCs-Exo-mediated liver protection, providing a promising therapeutic approach for improving liver graft outcomes.

Supplementary Information

The online version contains supplementary material available at https://doi.org/10.1186/s13287-025-04169-w.

Supplementary Material 1

Acknowledgements
The authors declare that they have not used Artificial Intelligence in this study.

Author contributions
SY and YJ conceived and designed the hypotheses of this study. YT, MJ and NY performed the major experiments, drafting the article and revising the final manuscript. ZG performed in vivo experiments and analyzed the data. All authors have approved the final manuscript to be submitted.

Funding
This project was supported by the National Natural Science Foundation of China (No. 82000619).

Data availability
The datasets used and/or analyzed during the current study are available from the corresponding author on reasonable request.

Declarations

Ethics approval and consent to participate
All animal studies were approved by the Institutional Animal Care and Use Committee of the Second Affiliated Hospital, School of Medicine, Zhejiang University. The title of the approved project is: mesenchymal stem cells-derived exosomes attenuate mouse non-heart-beating liver transplantation through miR-17-5p-regulated Kupffer cell pyroptosis. The approval number is 2020 – 379 and the approval date is March 11, 2020. This study did not involve human studies.

Consent for publication
All authors confirm their consent for publication.

Competing of interests
The authors have no conflict of interest.

Received: 23 July 2024 / Accepted: 23 January 2025
Published online: 07 February 2025

References

1. Artru F, Trovato F, Morrison M, Bernal W, McPhail M. Liver transplantation for acute-on-chronic liver failure, the lancet. Gastroenterology & hepatology; 2024.
2. Bodzin AS, Baker TB. Liver transplantation today: where we are now and where we are going. Liver Transpl. 2018;24(11):1470–1475.
3. Zamora-Valdes D, Leal-Leyte P, Kim PT, Testa G. Fighting mortality in the Waiting list: liver transplantation in North America, Europe, and Asia. Ann Hepatol. 2017;16:480–6.
4. Mi S, Jin Z, Qiu G, Xie Q, Hou Z, Huang J. Liver transplantation in China: achievements over the past 30 years and prospects for the future. Biosci Trends. 2022;16:212–20.
5. Jiang Y, Miao X, Wu Z, Xie W, Wang L, Liu H, Gong W. Targeting SIRT1 synergistically improves the antitumor effect of JQ-1 in hepatocellular carcinoma. Heliyon. 2023;9:e22093.
6. Tian Y, Wang J, Wang W, Ding Y, Sun Z, Zhang Q, Wang Y, Xie H, Yan S, Zheng S. Mesenchymal stem cells improve mouse non-heart-beating liver graft survival by inhibiting Kupffer cell apoptosis via TLR4-ERK1/2-Fas/FasL-caspase3 pathway regulation. Stem Cell Res Ther. 2016;7:157.
7. Vivalda S, Zhengbin H, Xiong Y, Liu Z, Wang Z, Ye Q. Vascular and biliary complications following deceased Donor Liver transplantation: a Meta-analysis. Transpl Proc. 2019;51:823–32.
8. Khalil A, Quaglia A, Gélat P, Saffari N, Rashidi H, Davidson B. New developments and challenges in Liver Transplantation. J Clin Med. 2023;12.
9. Wang L, Li J, He S, Liu Y, Chen H, He S, Yin M, Zou D, Chen S, Luo T, Yu X, Wan X, Huang S, Guo Z, He X. Resolving the graft ischemia-reperfusion injury during liver transplantation at the single cell resolution. Cell Death Dis. 2021;12:589.
10. Sosa RA, Ahn R, Li F, Terry AQ, Qian Z, Bhat A, et al. Myeloid spatial and transcriptional molecular signature of ischemia-reperfusion injury in human liver transplantation. Hepatol Commun. 2024;8.
11. Liu Y, Lou G, Li A, Zhang T, Qi J, Ye D, Zheng M, Chen Z. AMSC-derived exosomes alleviate lipopolysaccharide/d-galactosamine-induced acute liver failure by mir-17-mediated reduction of TXNIP/NLRP3 inflammasome activation in macrophages. EBioMedicine. 2018;36:140–50.
12. Jorgensen I, Miao EA. Pyroptotic cell death defends against intracellular pathogens. Immunol Rev. 2015;265:130–42.
13. Fang Y, Tian S, Pan Y, Li W, Wang Q, Tang Y, Yu T, Wu X, Shi Y, Ma P, Shu Y. Pyroptosis: a new frontier in cancer. Volume 121. Biomedicine & pharmacotherapy = Biomedecine & pharmacotherapie; 2020. p. 109595.
14. Frank D, Vince JE. Pyroptosis versus necroptosis: similarities, differences, and crosstalk. Cell Death Differ. 2019;26:99–114.
15. Li X, Wu Y, Zhang W, Gong J, Cheng Y. Pre-conditioning with tanshinone IIA attenuates the ischemia/reperfusion injury caused by liver grafts via regulation of HMGB1 in rat kupffer cells. Volume 89. Biomedicine & pharmacotherapy = Biomedecine & pharmacotherapie; 2017. pp. 1392–400.
16. Vande Walle L, Lamkanfi M. Drugging the NLRP3 inflammasome: from signalling mechanisms to therapeutic targets, Nature reviews. Drug Discovery. 2024;23:43–66.

17. Ni L, Chen D, Zhao Y, Ye R, Fang P. Unveiling the flames: macrophage pyroptosis and its crucial role in liver diseases. Front Immunol. 2024;15:1338125.
18. Guo W, Liu W, Chen Z, Gu Y, Peng S, Shen L, Shen Y, Wang X, Feng GS, Sun Y, Xu Q. Tyrosine phosphatase SHP2 negatively regulates NLRP3 inflammasome activation via ANT1-dependent mitochondrial homeostasis. Nat Commun. 2017;8:2168.
19. Yang S, Zhang Y, Peng Q, Meng B, Wang J, Sun H, Chen L, Dai R, Zhang L. Regulating pyroptosis by mesenchymal stem cells and extracellular vesicles: a promising strategy to alleviate intervertebral disc degeneration. Volume 170. Biomedicine & pharmacotherapy = Biomedecine & pharmacotherapie; 2024. p. 116001.
20. Yousefi AM, James PF, Akbarzadeh R, Subramanian A, Flavin C, Oudadesse H. Prospect of Stem Cells in Bone Tissue Engineering: A Review, Stem cells international, 2016 (2016) 6180487.
21. Kallekleiv M, Larun L, Bruserud Ø, Hatfield KJ. Co-transplantation of multipotent mesenchymal stromal cells in allogeneic hematopoietic stem cell transplantation: a systematic review and meta-analysis. Cytotherapy. 2016;18:172–85.
22. Suk KT, Yoon JH, Kim MY, Kim CW, Kim JK, Park H, Hwang SG, Kim DJ, Lee BS, Lee SH, Kim HS, Jang JY, Lee CH, Kim BS, Jang YO, Cho MY, Jung ES, Kim YM, Bae SH, Baik SK. Transplantation with autologous bone marrow-derived mesenchymal stem cells for alcoholic cirrhosis: phase 2 trial. Hepatology (Baltimore MD). 2016;64:2185–97.
23. Naji A, Eitoku M, Favier B, Deschaseaux F, Rouas-Freiss N, Suganuma N. Biological functions of mesenchymal stem cells and clinical implications, Cellular and molecular life sciences. Volume 76. CMLS; 2019. pp. 3323–48.
24. Damania A, Jaiman D, Teotia AK, Kumar A. Mesenchymal stromal cell-derived exosome-rich fractionated secretome confers a hepatoprotective effect in liver injury. Stem Cell Res Ther. 2018;9:31.
25. Kusuma GD, Carthew J, Lim R, Frith JE. Effect of the Microenvironment on Mesenchymal Stem Cell Paracrine Signaling: opportunities to engineer the Therapeutic Effect. Stem Cells Dev. 2017;26:617–31.
26. Zhao T, Sun F, Liu J, Ding T, She J, Mao F, Xu W, Qian H, Yan Y. Emerging role of mesenchymal stem cell-derived exosomes in Regenerative Medicine. Curr Stem Cell Res Therapy. 2019;14:482–94.
27. Liu M, Liu X, Su Y, Li S, Chen Y, Liu A, Guo J, Xuan K, Qiu X. Emerging role of mesenchymal stem cell-derived extracellular vesicles in oral and craniomaxillofacial tissue regenerative medicine. Front Bioeng Biotechnol. 2022;10:1054370.
28. Qiu G, Zheng G, Ge M, Wang J, Huang R, Shu Q, Xu J. Mesenchymal stem cell-derived extracellular vesicles affect disease outcomes via transfer of microRNAs. Stem Cell Res Ther. 2018;9:320.
29. Liang X, Ding Y, Zhang Y, Tse HF, Lian Q. Paracrine mechanisms of mesenchymal stem cell-based therapy: current status and perspectives. Cell Transplant. 2014;23:1045–59.
30. Gustafson HH, Holt-Casper D, Grainger DW, Ghandehari H. Nanoparticle uptake: the Phagocyte Problem. Nano Today. 2015;10:487–510.
31. Haga H, Yan IK, Takahashi K, Matsuda A, Patel T. Extracellular vesicles from bone marrow-derived mesenchymal stem cells improve survival from Lethal hepatic failure in mice. Stem Cells Translational Med. 2017;6:1262–72.
32. Fan G, Li Y, Chen J, Zong Y, Yang X. DHA/AA alleviates LPS-induced kupffer cells pyroptosis via GPR120 interaction with NLRP3 to inhibit inflammasome complexes assembly. Cell Death Dis. 2021;12:73.
33. Zhen H, Hu Y, Liu X, Fan G, Zhao S. The protease caspase-1: activation pathways and functions. Biochem Biophys Res Commun. 2024;717:149978.
34. Qian X, Jin P, Fan K, Pei H, He Z, Du R, Cao C, Yang Y. Polystyrene microplastics exposure aggravates acute liver injury by promoting Kupffer cell pyroptosis. Int Immunopharmacol. 2024;126:111307.
35. Kimura Y, Tamasawa N, Matsumura K, Murakami H, Yamashita M, Matsuki K, Tanabe J, Murakami H, Matsui J, Daimon M. Clinical significance of determining plasma MicroRNA33b in type 2 Diabetic patients with Dyslipidemia. J Atheroscler Thromb. 2016;23:1276–85.
36. Hu J, Jiang Y, Wu X, Wu Z, Qin J, Zhao Z, Li B, Xu Z, Lu X, Wang X, Liu X. Exosomal mir-17-5p from adipose-derived mesenchymal stem cells inhibits abdominal aortic aneurysm by suppressing TXNIP-NLRP3 inflammasome. Stem Cell Res Ther. 2022;13:349.
37. Liu S, Tang G, Duan F, Zeng C, Gong J, Chen Y, Tan H. MiR-17-5p inhibits TXNIP/NLRP3 inflammasome pathway and suppresses pancreatic β-Cell pyroptosis in Diabetic mice. Front Cardiovasc Med. 2021;8:768029.
38. Vidgren M, Oniscu GC. Liver transplantation from uncontrolled DCD donors-Is there light at the end of the tunnel? Liver Transplantation: Official Publication Am Association Study Liver Dis Int Liver Transplantation Soc. 2024;30:6–7.
39. Ruch B, Kumm K, Arias S, Katariya NN, Mathur AK. Donation after circulatory death liver transplantation: early challenges, clinical improvement, and future directions. Surg Clin North Am. 2024;104:27–44.
40. Ferguson SW, Wang J, Lee CJ, Liu M, Neelamegham S, Canty JM, Nguyen J. The microRNA regulatory landscape of MSC-derived exosomes: a systems view. Sci Rep. 2018;8:1419.

Publisher's note